

Dimensions and Forms of Artefacts in 1.5T and 3T MRI Caused by Cochlear Implants

Timo Maria Gottfried

Innsbruck Medical University

Daniel Dejaco

Innsbruck Medical University

Natalie Fischer

Innsbruck Medical University

Veronika Innerhofer

Innsbruck Medical University

Lejo Chacko

Innsbruck Medical University

Gerlig Widmann

Innsbruck Medical University

Christian Kremser

Innsbruck Medical University

Herbert Riechelmann

Innsbruck Medical University

Joachim Schmutzhard (✉ Joachim.Schmutzhard@i-med.ac.at)

Innsbruck Medical University

Research Article

Keywords: Artefacts, Cochlear implant, Magnetic Resonance Imaging, Dimensions

Posted Date: October 22nd, 2021

DOI: <https://doi.org/10.21203/rs.3.rs-668498/v1>

License:  This work is licensed under a Creative Commons Attribution 4.0 International License.

[Read Full License](#)

Abstract

Introduction:

Cochlear implantation is a standard treatment option due to expanding indications. Cranial magnetic resonance imaging (cMRI) has become a widespread diagnostic tool. Therefore, an increased number of cochlear implant (CI) users are undergoing cMRI scans. This study aimed to investigate the issue of the CI magnet impacting MRI quality and artifacts.

Material and Methods:

1.5T and 3T MRI scans with 4 defined sequences (T2-TSE, T2-TIRM, T1-3D-MPRAGE, and TDI) were performed on a phantom with a CI (Synchrony® System by MEDEL Austria®) in place. The resulting MRI artifacts were retrospectively compared to MRI artifacts observed in patients with a CI. All images were transferred to Amira® and visualized by manual segmentation.

Results:

Usable image quality was achieved in three sequences (T2-TSE, T2-TIRM and T1-mprage). Observed artifacts differed in shape and size depending on the sequence. Maximum diameters of fully extinguished areas ranged from 58x108x98 mm to 127x123x153 mm. Image distortions were larger.

Conclusion:

MRI artifacts caused by the Synchrony® system are asymmetric with varying shape, depending on the sequence. The phantom artefacts are similar to those in CI users. Considering the observed asymmetry, the hypothesis of varying implantation locations resulting in varying positions of the signal void area needs to be further investigated.

Introduction

Cochlear implantation has developed into a standard treatment option for patients with severe to profound hearing loss. [1, 2] The number of patients treated with a cochlear implant (CI) rose from approx. 110,000 patients in 2008 [1] to over 400,000 patients in 2017 [3] worldwide. This rapid development was driven by an extension of the CI indication criteria which now cover all age groups ranging from newborns to elderly people with hearing loss. [4] The rising number of patients and the higher age of CI recipients increase the likeliness that CI users will require cranial imaging modalities after cochlear implantation.

Cranial magnetic resonance imaging (cMRI) is frequently used in the diagnostic work-up of neurological [5, 6] and otologic diseases [7, 8]. The increasing indications for cMRI, better availability, and lower examination cost have led to an increased implementation of cMRI worldwide. [9]

As a consequence, the number of cMRI scans in CI users is also increasing. MRI scans in this cohort are still subject to certain limitations, e.g. pain, heat development, demagnetization, and dislocation of the inner magnet [10-13]. The safety limitations are directly linked to the magnetic field strength measured in Tesla (T). Therefore, MRI-compatible CI systems approved for up to 3T MRI scans were developed by different manufacturers[14, 15].

Nonetheless, also these innovative CIs contain metallic and magnetic components which cause artifacts in cMRI scans and thus decrease their diagnostic value. The artifacts vary in size and shape depending on magnetic field strength, cMRI sequence, and position of the internal CI magnet [16-18].

At 3T, artifacts caused by the CI have been shown to affect image quality of the nearby brain regions depending on the chosen sequence. Majdani et al. (2009) observed additional periodic shadowing especially in T2-weighted sequences in 3T cMRI performed with one phantom and three cadaveric specimens. The authors concluded that these artifacts reduce the likeliness of accurate diagnosis of brain lesions on the ipsilateral side [18].

In a retrospective chart review in 2016, Sharon et al. evaluated 57 MRI brain scans of CI users. This analysis revealed several factors influencing the image quality with a CI magnet in situ. One main factor influencing the size and shape of the artifact was the MRI sequence used. [19]

This observation was further scrutinized by Edmonson et al. Their findings support the hypothesis of a correlation between the expected artifact and the applied MRI sequences [20]. Furthermore a non-symmetric shape of these artifacts has been discussed [19]. However, these three-dimensional shapes have yet to be described depending on the MRI sequence and magnetic field strength applied.

The aim of this study was to visualize and quantify artifacts caused by a specific cochlear implant system (MED-EL Synchrony®) in frequently used cMRI sequences in 1.5T and 3T magnetic fields. Artifact visualization and size measurement was performed using a specific MRI phantom.

Materials And Methods

The 3T images were acquired using a whole body MRI scanner (Magnetom Skyra, Siemens, Erlangen; Germany); the 1.5 images were acquired using a Magnetom Avanto (Siemens, Erlangen; Germany).

The sequences were chosen according to the in-house protocol for cerebellopontine angle imaging including: 1) T2-weighted turbo spin echo (T2-TSE), 2) T2-weighted Turbo inversion recovery with magnitude reconstruction (T2-TIRM) and 3) T1-weighted 3D-magnetization-prepared rapid gradient echo (3D-MPRAGE)[21], 4) diffusion tensor imaging sequence (DTI). Sequence parameters are listed in Table 1.

MRI with the above sequences was performed using a special MRI phantom which had been prepared with a MEDEL Synchrony® CI. Furthermore, retrospective analysis of MRI images of CI users from the local database was performed. The artifacts were visualized as 3D models to enable exact metric measurement and 3D modeling.

MRI phantom:

The Phantom was used in accordance with Majdani O's study from 2009.¹⁸ 10-mm-thick Plexiglas plates with 5x5 mm grids were stacked on top of each other. The grids on each layer were placed on top of each other, so that each grid element formed a 5x5x5mm cube resulting in a total volume of 17cmx17 cm. This 3D grid allowed a quantification of the artifacts and distortions caused by a MED-EL Synchrony CI.

Different experiment setups were conducted. First, the CI was placed on a lateral location, simulating a real device implanted on a human head. Second, the individual components of a CI (magnet and implant without magnet) and the complete device were placed in the center of the phantom to investigate the full dimensions of the artifact and which part of the CI is responsible for it.

To obtain an MRI signal, the phantom was filled with 3 liters of 0.9% saline solution. The prepared phantom was then placed in the standard 20-channel head coil of the MRI scanner and imaging using the sequences listed above was performed.

Retrospective MRI images:

A retrospective search of the hospital MRI database for cMRI images with CIs was performed. After defining critical anatomic landmarks, these images were evaluated by an in-house radiologist for their quality and readability with special regard to the above listed sequences.

All procedures performed in studies involving human participants were in accordance with the ethical standards of the institutional and/or national research committee and with the 1964 Helsinki Declaration and its later amendments or comparable ethical standards. Informed consent for the scientific use of performed images was obtained from all individual participants included in the study. *Because of the retrospective character of the study, the Ethics Committee of the Medical University of Innsbruck certified that no ethics committee approval is required under Austrian law.*

Data visualization:

DICOM data from the phantom examinations and the retrospective search were transferred into Amira® (Thermo-Fisher Scientific-Fei Visualization Science Group, Méignac Cédex, France). This software contains tools for 3D rendering, measurement, and defining (Figure 1).

Using this program, each slice of the MRI scans was manually segmented twice, following Glueckert et al. [22], creating a 3D model of a) the fully extinguished areas and b) areas of distortion for each individual sequence.

Finally, the dimensions of these 3D models were measured using Amira® and transferred to Microsoft Excel files.

Results

The following MRI sequences were used with the phantom: T2-TSE, T2-TIRM, 3D-MPRAGE and DTI. The acquired images were evaluated for possible usability. All diffusionweighted images were excluded due to poor quality and classified as not readable.

T2-TSE, T2-TIRM and 3D-MPRAGE sequences were assessed as readable, providing partially usable information. The images obtained with these sequences were manually segmented using the Amira visualization program as described above.

T2-weighted turbo spin echo:

In the phantom with a laterally placed CI, the T2-TSE sequence in 3T MRI resulted in signalvoid areas with the following measurements: 66 mm in coronary, 117 mm in sagittal and 98 mm in axial dimension (Table 2). The extent of the distorted area in a 3T magnetic field was 94x135x145 mm (Table 3) (Figure 2).

The measurements of the individual CI components placed in the center of the phantom model (Figure 2) with T2-TSE sequences resulted in a signal-void artifact of 26x46x43 mm for the casing, 121x97x122 mm for the magnet and 123x96x128 mm for the complete CI (Table 4). The maximum extent of distorted areas was 139x148x135 mm for the sole magnet, 50x66x60 mm for the casing, and 151x128x146 mm for the complete CI (Figure 3).

Segmented signal void artifacts in the retrospectively analyzed MRI images of CI users were 58x107x92 mm in 1.5T and 63x103x121 mm in 3T fields. Distorted areas extended to a maximum of 66x125x103 mm using 1.5T and 74x146x102 mm using 3T (Figure 4).

T2-weighted turbo inversion recovery magnitude:

Applying 3T TIRM-Imaging on the phantom with a laterally placed CI, fully extinguished areas measured 121x117x136 mm (Figure 2).

According to the T2-TSE protocol, the CI and its components were placed individually in the center of the model and 3T TIRM-imaging was conducted for each of them. Their segmented artifacts showed a maximum dimension of 151x172x150 mm (CI), 159x170x152 mm (magnet) and 66x26x75 mm (casing) (Figure 3).

Extinguished areas in the retrospectively segmented CI user data measured 127x123x153 mm in a 1.5T and 121x117x136 in a 3T magnetic field (Figure 4).

T2-TIRM sequences generated distorted areas of a greater extent than the used model and were therefore excluded from this study as they were unmeasurable.

T1-weighted 3D magnetization-prepared rapid gradient echo sequence:

Applying the T1-3D-MPRAGE sequence on the phantom in 3T condition, the artifact measured 88x122x140 mm in the signal-void area and 174x154x140 mm in the distorted area (Figure 2).

The individual components caused artifacts with a size of 127x127x129 mm for the complete CI, 129x134x135 mm for the magnet, and 38x44x51 mm for the casing. Distorted areas measured 150x139x144 mm (CI) and 137x134x139 mm (magnet) (Figure 3).

The retrospective data showed artifacts of 74x155x115 mm at 1.5T and 62x114x83 mm at 3T. The maximum extent of distorted areas was 85x161x110mm at 1.5T and 120x200x142 mm at 3T (Figure 4).

Furthermore, the data was reviewed by an in-house radiologist to evaluate the use of image quality and readability. Focus was the clinical use and assessability of important anatomic structures like medulla oblongata, inner ear, cerebellar bridge angle, as well as cerebrospinal fluid space and the cerebellum. In general, all T2 TSE sequences provided a distinctly better visualization of the inner head compartments compared to the T1-mp_rage sequences (Figure 5 a-b). Only the cerebrospinal fluid spaces were comparable in their radiological value. (Figure 5 c-d) T2-TIRM sequenced images provided nearly the same image quality and visualization of critical anatomic landmarks as T2 TSE sequences. Merely the assessment of the inner ear canal was clearly better in T2 TSE sequences.

Discussion

All types of implants with metallic and magnetic components are well known to cause artifacts in MRI scans. The potential of CIs to cause artifacts in MRI scans has been described in multiple publications.¹⁷⁻²⁰ In this study, the artifacts caused by the Synchrony® CI system (MEDEL, Austria) were visualized using MRI phantom trial images and MRI images of CI users. The observed artifacts differed in shape, size, and symmetry depending on the sequences used.

When applying a standard cMRI protocol, a primary differentiation between readable and unreadable sequences needs to be made. All diffusion sequences (ADC, tracer-weighted, and tensor diffusion-weighted) were unreadable with the magnet in place. This observation was previously published by Edmonson et al who described diffusion-weighted sequences with significant geometric distortion and intravoxel dephasing [20]. As concluded by Edmonson et al. and also confirmed in the present study, the usability and necessity of diffusion-weighted images with the CI magnet in place must be scrutinized and might be dispensable.

T2 TSE, T1 MP_RAGE and T2 TIRM were classified as partly readable with varying size, shape, and quality of the artifact. A signal-void area, which comprised a black unreadable area close to the magnet, could be distinguished from a distortion area with partly distorted but readable visual information.

Different shapes depending on the used sequence and magnet strength were observed in the phantom pictures and real patient pictures. The T2 TSE sequence visualized a chalice-like signal-void area with a surrounding distortion area. The T1 MP-RAGE sequence visualized a spinner-like signal-void area with a

small distal tip and proximal widening and a surrounding distortion area. The T2 TIRM sequence did not show a distortion area. The signal void region in the cross section had a flower-like structure (Figure 2 a-i).

These asymmetries seem to depend on the special and unique structure of the CI itself. The artifacts were identical in the phantom pictures and the patient pictures (Figure 2 and 4). The different shapes, however, may provide opportunities regarding their location in relation to the different anatomical structures. It should be possible to influence their location by changing the implantation angle or distance to the inner ear. This indicates that it could be possible to position the CI in a way that favors MRI scans of important intracerebral structures, e.g., the brainstem or the corpus callosum.

Ingo Todt and colleagues assessed this hypothesis to some extent. In a recent study, Todt et al (2015) tested different implant locations with regard to insertion angles (90° , 120° and 160°) and distance to the inner ear (5cm, 7cm and 9cm). Then 3T MRI was applied. [23] Their results show a clearly better visualization of the inner ear canal and cerebral structures with the CI being located farther away (9cm) and with a higher insertion angle (120°). This further verifies the assumption above. In 2018, Dirk Schröder and colleagues carried out a study with a very similar protocol using 1.5 MRI. Their results correspond with the previous studies. [24] However, in both study protocols they fixed the CI onto the head with a tight dressing and did not proceed an implantation. Therefore, further studies are required to further confirm this hypothesis and change the standard implant location.

Applying 1.5T and 3T scans, this study revealed smaller artifacts in 1.5T examinations than in 3.0T scans. (Figure 5 e-f) Using T2-weighted TSE sequences, artifacts were 7-10 mm smaller in the 1.5T examinations than in the 3T examinations. Using T1-weighted multiplanar sequences, the difference between 1.5 and 3T goes up from 12 to 43 millimeters. Based on this observation, 1.5T examinations should be preferred when imaging the head with a CI magnet in place to enable better visualization of the central brain structures.

This differs from the results Omid Majdani and colleagues (2009) found in their trial using the same study modalities as in the present study with prior MED-EL implant systems. They concluded that the artifacts produced in 1.5T and 3T MRI scans are about the same size and have no significant variance [18]. The difference between the outcomes of the study and Majdani's et al.'s study can be explained with the further developed visualization technique applied in the present study.

In addition to the described magnet strength depending size difference discussed above an MRI sequence depending size variance can be observed as well. The T2-weighted turbo spin echo sequences produce significant smaller artifacts than T1-weighted mp_rage sequences. Therefore, the anatomical T2 TSE modality seems to be a favorable choice for anatomical cMRI examinations with the CI magnet in place. This finding matches the results of a previously published paper by Omid Majdani in 2008 regarding artifacts caused by CIs in 3T MRI scans [18]. However, the maximum dimensions of the artifacts visualized in this study are up to 10 mm larger with the SYNCHRONY® CI than with the PULSAR® CI used in the 2008 publication. A possible explanation could be the different composition of

the magnets. The PULSAR® CI magnet consists of a samarium-cobalt whereas the SYNCHRONY® CI consists of a neodymium iron boron mixture. In addition, shear force direction differs between the two magnets. However, the magnetic field strength is identical in both CI models. Additionally, both studies are a decade apart and therefore image quality and the number of images per unit may differ due to technical improvement of MRI scans. This could possibly be another reason for the varying results.

The phantom MRI scan performed with a separate magnet and a Synchrony CI without the magnet in situ revealed the expected results. The magnet is responsible for nearly the entire artifact caused by a CI in MRI scans. As depicted in Table 3, the casing alone generates an artifact of 2.5 to 5 cm in maximum diameter whereas the magnet itself produces artifacts of up to 15 cm. Artifacts solely produced by the magnet led to the typical shapes described above, depending on the sequence applied. Whereas performing those sequences on just the casing resulted in symmetrical artifacts with no comparability to any shape described above.

These results support an experimental human cadaver study by Franca Wagner and colleagues in 2015 showing that the removal of the internal magnet can significantly reduce the size of artifacts caused by a CI in MRI scans. [25] In one retrospective case, a patient had a CI implanted on both sides; and as depicted in Figure 4, the shape and position of the resulting artifact does not depend on the side of surgery. In fact, both artifacts could be mirrored about a sagittal plane between the brain hemispheres. This means that the maximum and minimum extent of the artifact on each side are located at the same height and position of the head and therefore mask the same anatomic structures. The main reason for the caused unreadable area is the magnet as mentioned above. One explanation for this might be that the magnet of the MED-EL Synchrony® is rotatable and can therefore reposition in the magnetic field. There are no recent studies to support this hypothesis. Further investigation needs to be conducted to verify this theory.

Conclusion

Artifacts in MRI scans caused by the Synchrony CI system vary in shape and size depending on the sequences applied. Furthermore, the artifact shape is asymmetrical inside human head tissue. With this observed asymmetry, the hypothesis of varying implantation locations resulting in varying positions of the signal void area needs to be further investigated. It seems possible to visualize intracerebral structures by changing the implantation area or insertion angle. Further studies are needed to verify this conclusion.

Abbreviations

Abbreviation	Full Form
CI	Cochlea Implant
cMRI	Cranial magnetic resonance imaging
T	Tesla
T2_TSE	T2-weighted turbo spin echo
T2-TIRM	T2-weighted turbo inversion recovery with magnitude reconstruction
T1_MPRAGE	T1-weighted 3D magnetization prepared rapid gradient echo
DTI	Diffusion tensor imaging

Declarations

Funding: No funds or payments were received by any contributing author regarding this study

Conflicts of interest: The corresponding author received research funds from the the R&D Department of MED-EL Elektromedizinische Geräte GmbH Innsbruck

Availability of data and material: All data regarding this study is available.

Code availability: not applicable.

Acknowledgement:

We would particularly like to thank Martin Zimmerling from the R&D Department of MED-EL Elektromedizinische Geräte GmbH Innsbruck for kindly providing us with the phantom model and the MED-EL Synchrony cochlear implant used in this study. We would also like to thank Ursula Lehner-Mayrhofer from the Clinical Research Department of MED-EL Elektromedizinische Geräte GmbH Innsbruck for performing a language edit on a version of this manuscript.

References

1. Fallon JB, Irvine DRF, Shepherd RK. Cochlear implants and brain plasticity. *Hear Res*. 2008;238(1-2):110-7. doi:10.1016/j.heares.2007.08.004.
2. US Department of Health & Human Services NIoDaOCD. Cochlear Implants. 2017.
3. Todt I, Tittel A, Ernst A, Mittmann P, Mutze S. Pain Free 3 T MRI Scans in Cochlear Implantees. *Otolaryngology & Neurotology*. 2017;38(10):e401-e4. doi:10.1097/mao.0000000000001569.
4. Stark T, Helbig S. [Cochlear implantation: a changing indication]. *Hno*. 2011;59(6):605-14. doi:10.1007/s00106-011-2309-9.

5. Xiang X, Cao F. Time window and "tissue window": two approaches to assist decision-making in strokes. *J Neurol*. 2019;266(2):283-8. doi:10.1007/s00415-018-8933-5.
6. Chen X, Liu Y, Tong H, Dong Y, Ma D, Xu L et al. Meta-analysis of computed tomography angiography versus magnetic resonance angiography for intracranial aneurysm. *Medicine (Baltimore)*. 2018;97(20):e10771. doi:10.1097/MD.00000000000010771.
7. Lingam RK, Connor SEJ, Casselman JW, Beale T. MRI in otology: applications in cholesteatoma and Meniere's disease. *Clin Radiol*. 2018;73(1):35-44. doi:10.1016/j.crad.2017.09.002.
8. Forgues M, Mehta R, Anderson D, Morel C, Miller L, Sevy A et al. Non-contrast magnetic resonance imaging for monitoring patients with acoustic neuroma. *J Laryngol Otol*. 2018;132(9):780-5. doi:10.1017/s0022215118001342.
9. Hartwig V, Giovannetti G, Vanello N, Lombardi M, Landini L, Simi S. Biological effects and safety in magnetic resonance imaging: a review. *Int J Environ Res Public Health*. 2009;6(6):1778-98. doi:10.3390/ijerph6061778.
10. Nospes S, Brockmann MA, Lassig A. [MRI in patients with auditory implants equipped with implanted magnets-an update : Overview and procedural management]. *Radiologe*. 2019;59(1):48-56. doi:10.1007/s00117-018-0462-9.
11. Kim BG, Kim JW, Park JJ, Kim SH, Kim HN, Choi JY. Adverse events and discomfort during magnetic resonance imaging in cochlear implant recipients. *JAMA Otolaryngol Head Neck Surg*. 2015;141(1):45-52. doi:10.1001/jamaoto.2014.2926.
12. Majdani O, Leinung M, Rau T, Akbarian A, Zimmerling M, Lenarz M et al. Demagnetization of cochlear implants and temperature changes in 3.0T MRI environment. *Otolaryngol Head Neck Surg*. 2008;139(6):833-9. doi:10.1016/j.otohns.2008.07.026.
13. Hassepass F, Stabenau V, Maier W, Arndt S, Laszig R, Beck R et al. Revision surgery due to magnet dislocation in cochlear implant patients: an emerging complication. *Otol Neurotol*. 2014;35(1):29-34. doi:10.1097/MAO.0b013e3182a5d2c5.
14. Limited C. MRI Guidelines. <https://www.cochlear.com/us/en/professionals/resources/mri-guidelines>. 2019. Accessed 27.03.2020.
15. MEDEL. MED-EL Announces FDA Approval of PULSAR, SONATA and MED-EL CONCERT Cochlear Implants for 1.5T MRI. https://s3.medel.com/pdf/US/Final_MRI_FDA_Approval_Press_Release_06_14_13.pdf 2013.
16. Carlson ML, Neff BA, Link MJ, Lane JI, Watson RE, McGee KP et al. Magnetic Resonance Imaging With Cochlear Implant Magnet in Place: Safety and Imaging Quality. *Otol Neurotol*. 2015;36(6):965-71. doi:10.1097/mao.0000000000000666.

17. Crane BT, Gottschalk B, Kraut M, Aygun N, Niparko JK. Magnetic resonance imaging at 1.5 T after cochlear implantation. *Otol Neurotol.* 2010;31(8):1215-20. doi:10.1097/MAO.0b013e3181ec1d61.
18. Majdani O, Rau TS, Gotz F, Zimmerling M, Lenarz M, Lenarz T et al. Artifacts caused by cochlear implants with non-removable magnets in 3T MRI: phantom and cadaveric studies. *Eur Arch Otorhinolaryngol.* 2009;266(12):1885-90. doi:10.1007/s00405-009-0994-8.
19. Sharon JD, Northcutt BG, Aygun N, Francis HW. Magnetic Resonance Imaging at 1.5 Tesla With a Cochlear Implant Magnet in Place: Image Quality and Usability. *Otol Neurotol.* 2016;37(9):1284-90. doi:10.1097/mao.0000000000001176.
20. Edmonson HA, Carlson ML, Patton AC, Watson RE. MR Imaging and Cochlear Implants with Retained Internal Magnets: Reducing Artifacts near Highly Inhomogeneous Magnetic Fields. *Radiographics.* 2018;38(1):94-106. doi:10.1148/rg.2018170135.
21. Mugler JP 3rd, Brookeman JR. Three-dimensional magnetization-prepared rapid gradient-echo imaging (3D MP RAGE). *Magn Reson Med.* 1990;15(1):152-7. doi:10.1002/mrm.1910150117.
22. Glueckert R, Johnson Chacko L, Schmidbauer D, Potrusil T, Pechriggl EJ, Hoermann R et al. Visualization of the Membranous Labyrinth and Nerve Fiber Pathways in Human and Animal Inner Ears Using MicroCT Imaging. *Front Neurosci.* 2018;12:501-. doi:10.3389/fnins.2018.00501.
23. Todt I, Rademacher G, Mittmann P, Wagner J, Mutze S, Ernst A. MRI Artifacts and Cochlear Implant Positioning at 3 T In Vivo. *Otol Neurotol.* 2015;36(6):972-6. doi:10.1097/mao.0000000000000720.
24. Schroder D, Grupe G, Rademacher G, Mutze S, Ernst A, Seidl R et al. Magnetic Resonance Imaging Artifacts and Cochlear Implant Positioning at 1.5 T In Vivo. *Biomed Res Int.* 2018;2018:9163285. doi:10.1155/2018/9163285.
25. Wagner F, Wimmer W, Leidolt L, Vischer M, Weder S, Wiest R et al. Significant Artifact Reduction at 1.5T and 3T MRI by the Use of a Cochlear Implant with Removable Magnet: An Experimental Human Cadaver Study. *PLoS One.* 2015;10(7):e0132483. doi:10.1371/journal.pone.0132483.

Tables

Table 1: Image specifications

	T2-TSE	T2-TIRM	3D-MPRAGE	DTI
TR (ms)	5800	8000	7.8	7000
TE (ms)	95	87	2.94	95
TI (ms)	-	2370	1100	-
Flip angle	90° / 150°	90° / 150°	8°	90
Echo train length	16	16	1	64
Pixel bandwidth (Hz/Px)	220	250	250	1500
Acquisition matrix	218 x 384	175 x 320	187 * 256	64 x 128
Reconstructed matrix	312 x 384	250 x 320	208 x 256	256 x 256
Field of view (mm)	178 x 220	171 x 220	178 x 220	220 x 220
Slice thickness (mm)	2	3	1	3
Gap between slices (mm)	0	0.6	0	0,3
Number of slices	75	45	176	43
Number of concatenations	3	2	1	1
Parallel imaging mode	GRAPPA	-	GRAPPA	GRAPPA
Parallel imaging factor	2	-	2	2
Number of diffusion encoding directions	-	-	-	20
b-value	-	-	-	1000
Voxel size (mm)	0.573 x 0.573 x 2	0.688 x 0.688 x 3	0.859 x 0.859 x 1	0.859 x 0.859 x 3
Acquisition time	3 * 54.40 sec	2 * 1min 20sec	3min 36sec	2min 50sec

TR (ms): repetition time (in milliseconds), **TE:** echo time, **TI:** inversion time,

Hz/Px: Herz per pixel, **MM:** millimeter

Table 2: Maximum extent of extinguished areas in mm

Sequences	Coronary	Axial	Sagittal
------------------	-----------------	--------------	-----------------

Phantom 3T Extinguished:			
T2-TSE	66	117	98
T2-Tirm	121	117	136
T1 mp_rage	88	122	140
Patient 1.5T extinguished:			
T2-TSE	58	107	92
T2-Tirm	127	123	153
T1 mp_rage	74	155	115
Patient 3T extinguished:			
T2-TSE	63	103	121
T2-Tirm	121	117	136
T1 mp_rage	62	114	83

Table 3: Maximum extent of distorted areas in mm

Sequences	Coronary	Axial	Sagittal
------------------	-----------------	--------------	-----------------

Phantom 3T Distorted:

T2-TSE	94	135	145
---------------	----	-----	-----

T1 mp_rage	174	154	140
-------------------	-----	-----	-----

Patient 1.5T Distorted:

T2-TSE	66	125	103
---------------	----	-----	-----

T1 mp_rage	85	161	110
-------------------	----	-----	-----

Patient 3T Distorted:

T2-TSE	74	146	102
---------------	----	-----	-----

T1 mp_rage	120	200	142
-------------------	-----	-----	-----

Table 4: Dimensions of the extinguished areas individual components in mm

Sequences	Coronary	Axial	Sagittal
-----------	----------	-------	----------

Magnet 3T Extinguished:

T2-TSE	121	97	122
T2-Tirm	159	170	152
T1 mp_rage	129	134	135

Casing 3T Extinguished

T2-TSE	26	46	43
T2-Tirm	66	26	75
T1 mp_rage	38	44	51

CI 3 Tesla Extinguished:

T2-TSE	123	96	128
T2-Tirm	151	172	150
T1 mp_rage	127	127	129

Figures

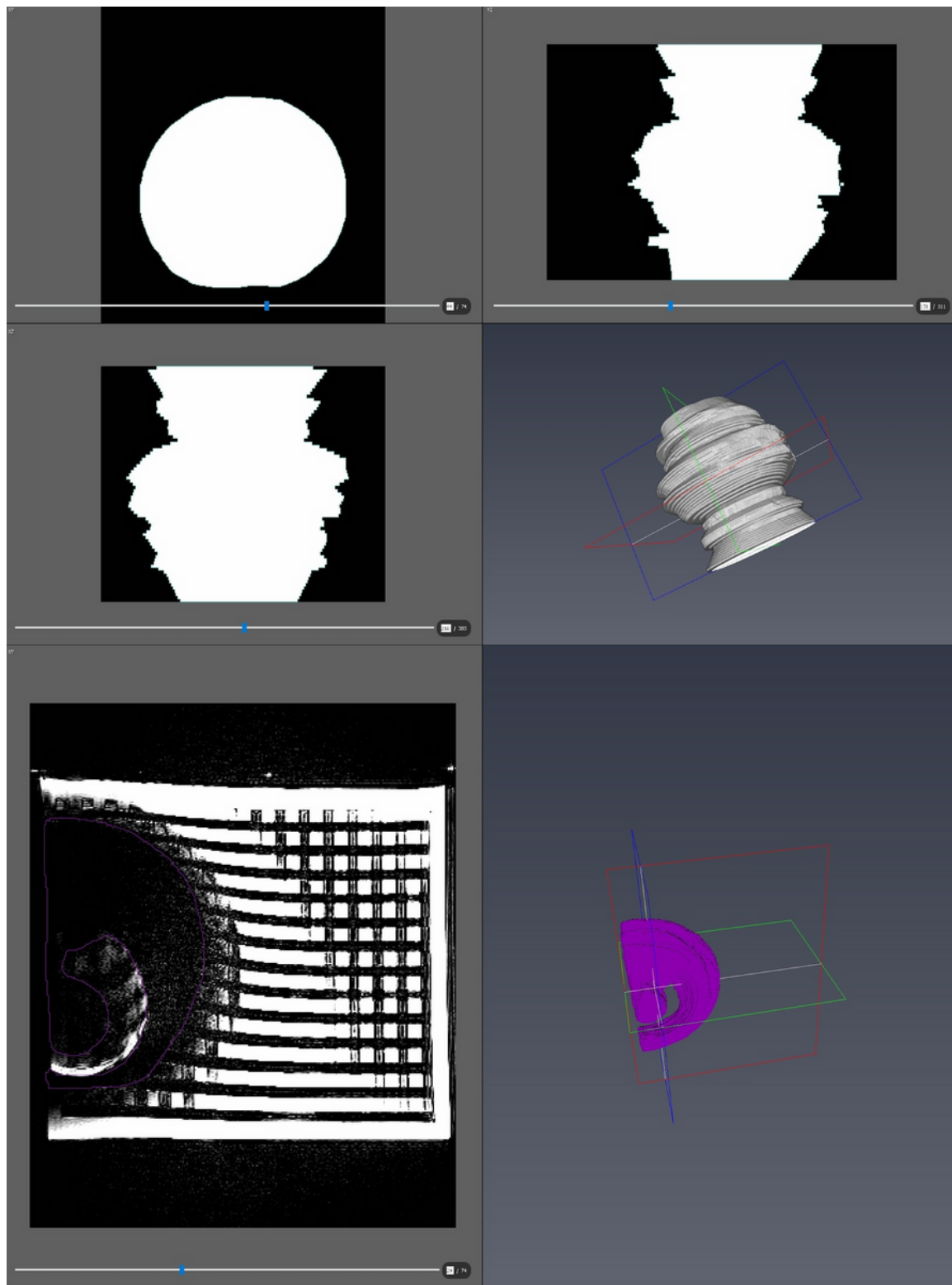


Figure 1

depicts the segmentation process using Amira software. Insert a) – c) depicts the 2-dimensional view which has been marked by hand. In d) the 3-dimensional composition gathered by a) – c) is visualized. Picture e) shows a T2-TSE sequence in the segmentation process. The extinguished area has been marked by hand in pink. Insert f) visualizes the resulting 3-D image.

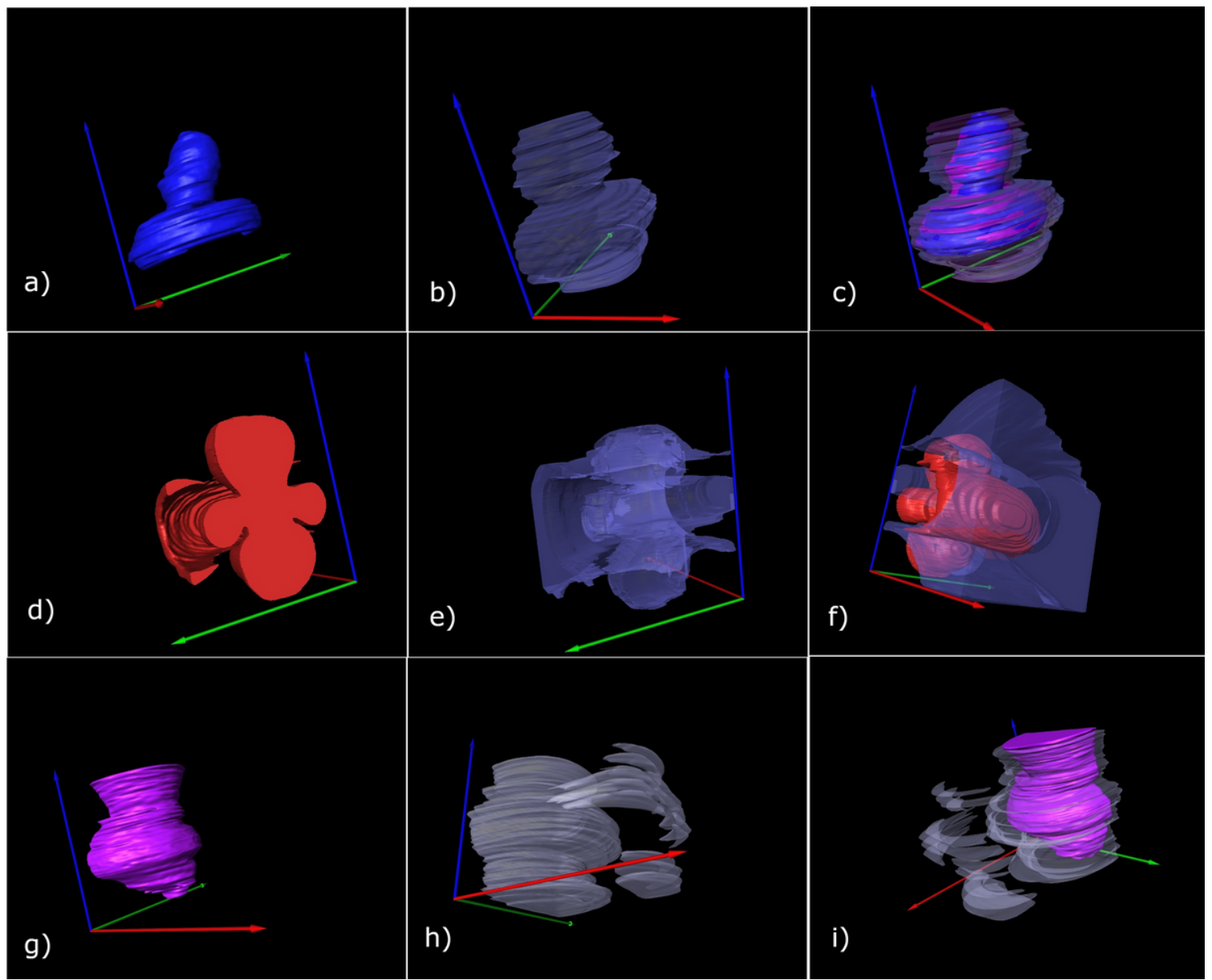


Figure 2

depicts the extinguished and distorted areas caused by a MED-EL Synchrony CI laterally placed on the phantom for each of the included sequences. Inserts a) – c) show the results for T2-TSE. The extinguished area is visualized in a, the distorted area in b). Picture c) shows the combination of a) and b). the pink and blue coloring shows results of two different segmentations, which appear to be identical. In picture d) – f) the T2-tirm sequence is presented with the extinguished area in d), the distorted area in e) and the combination in f). T1-mp_rage sequence is shown in g) – i) with the extinguished area in g), the distorted area in h) and the combination in i).



Figure 3

shows the 3D shapes of artifacts caused by the individual components – casing, magnet and the assembled system. Insert a) – c) visualize the T1-mp_rage sequence. The extinguished area caused by the casing is seen in a), b) visualizes the extinguished area caused by the magnet and c) the extinguished area caused by the assembled system. In d) – f) the T2-tirm sequence is presented – d) casing, e) magnet and f) assembled system. The pictures g) – i) show the results for the T2-TSE sequence with g) representing the casing, h) the magnet and i) the assembled system.

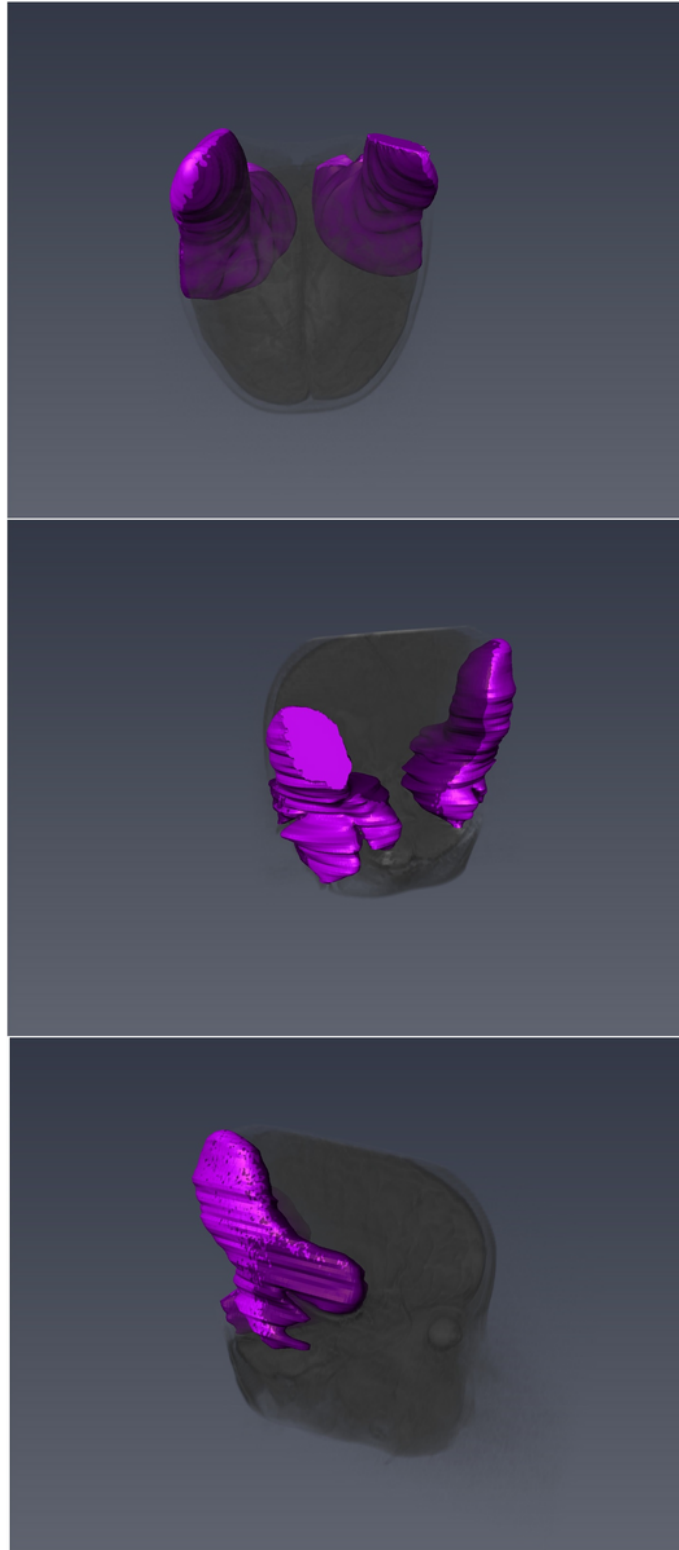


Figure 4

presents the position of the artifact in correlation to the human head. The example shows the typical T2-TSE sequence artifact in a 1.5T setting of a bilaterally implanted patient. The orientation of the artifact is mirrored.

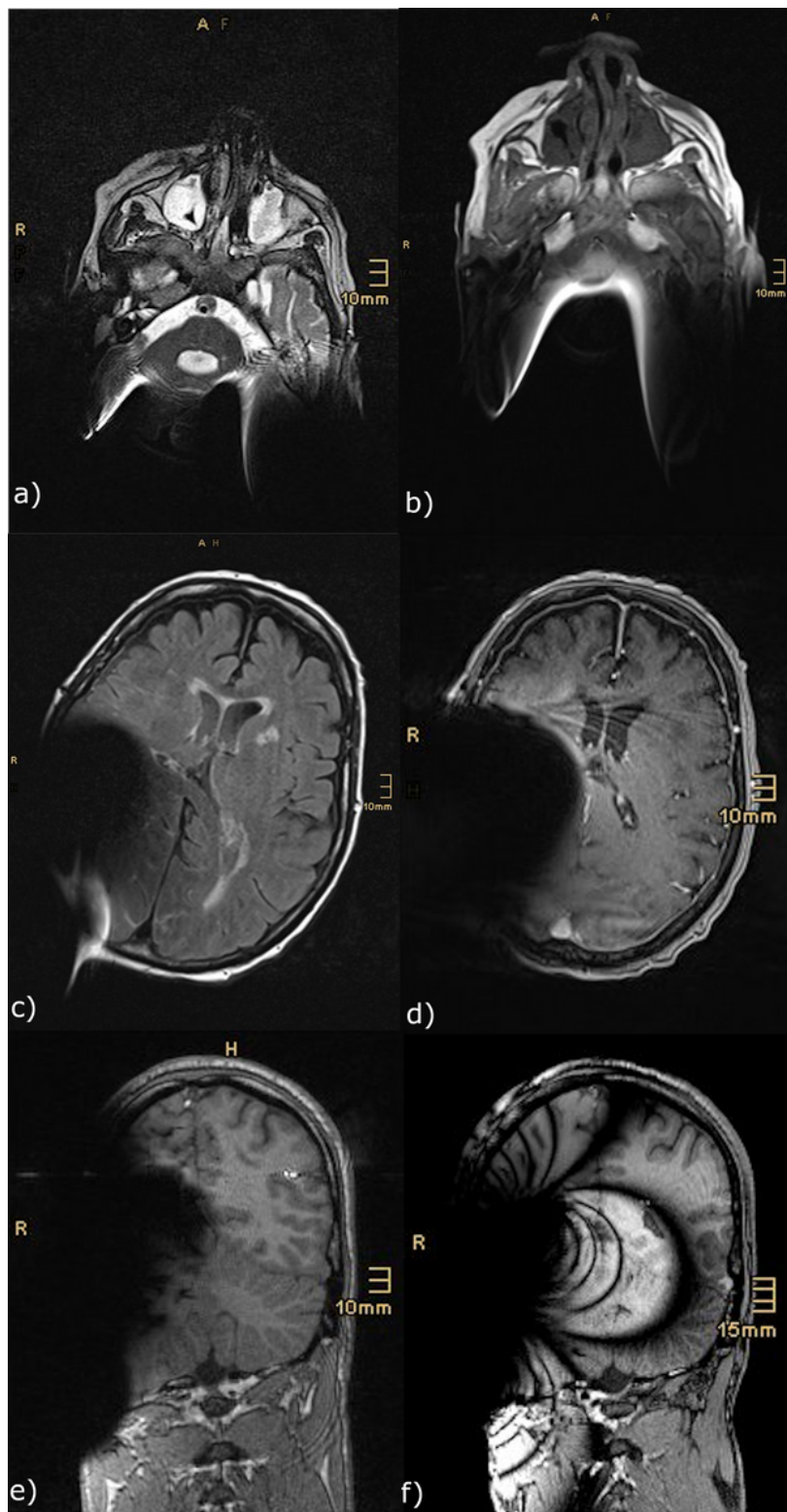


Figure 5

shows examples of the retrospective data used in this study. The pictures a) and c) present different layers of 1,5T T2 TSE sequences done in a patient with a cochlear implant on a) both sides and c) the

right side. Pictures b) and d) show a comparable layer of the same patient done in a T1-mp_rage sequence. Picture e) visualize exemplary an artefact caused by a CI on the right side in a 1,5T MRI (T1-mp_rage), while picture f) represents nearly the same layer of an image done in a 3T device.